Available online at www.sciencedirect.com
SCIENCE DIRECT
Journal of Power Sources 146 (2005) 496–500
JOURNAL OF POWER SOURCES
www.elsevier.com/locate/jpowsour

All-solid-state lithium secondary batteries with $SnS–P_2S_5$ negative electrodes and $Li_2S–P_2S_5$ solid electrolytes

Akitoshi Hayashi *, Takanori Konishi, Kiyoharu Tadanaga, Tsutomu Minami, Masahiro Tatsumisago

Department of Applied Chemistry, Graduate School of Engineering, Osaka Prefecture University, 1-1 Gakuen-cho, Sakai, Osaka 599-8531, Japan

Available online 2 June 2005

Abstract

The $80SnS·20P_2S_5$ (mol%) amorphous material was prepared by a mechanical milling technique. The obtained material was fine powders with a few micrometers in size. All-solid-state cells with the $SnS–P_2S_5$ amorphous electrode and the $Li_2S–P_2S_5$ glass-ceramic electrolyte, where a continuous P_2S_5 sulfide network between both the materials was formed, were fabricated. The cells exhibited high reversible capacity of over 400 mAh g^{-1} for 50 cycles at room temperature. The addition of P_2S_5 as a glass former to SnS improved cell capacity and cyclability, suggesting that P_2S_5 network played an important role in enhancing the availability of SnS as an electrode material.

Keywords: SnS; Anode; Lithium battery; Solid-state battery; Solid electrolyte

1. Introduction

Tin oxide-based glasses in the systems such as $SnO–B_2O_3–P_2O_5–Al_2O_3$ [1–4] have been extensively studied as a negative electrode material with high specific capacity for lithium secondary batteries. These glassy materials were prepared by conventional melt quenching and mechanical milling techniques. The latter technique has a great advantage of producing fine powders, which are directly applied to batteries, without an additional pulverizing procedure of bulk glasses. A room temperature operation is also a favorable factor of the mechanical milling process. We have succeeded in preparation of the oxide glassy powder in the systems $SnO–B_2O_3–P_2O_5$ [5], $SnO–B_2O_3$ [6], and $SnO–P_2O_5$ [7] by mechanical milling. These glasses worked as negative electrode materials for rechargeable lithium cells with conventional liquid electrolytes.

Nowadays, all-solid-state batteries with a solid electrolyte instead of a liquid electrolyte attract much attention because they have high reliability and safety. All-solid-state $In/LiCoO_2$ cells with a solid electrolyte in the system $Li_2S–P_2S_5$ showed great performance as a rechargeable lithium battery with high capacity and excellent cyclability at room temperature [8].

Novel tin sulfide-based glasses as a negative electrode would be compatible with the sulfide solid electrolytes in all-solid-state cells. Momma et al. have reported that amorphous and crystalline SnS_2 powders were electrochemically charged and discharged in the cells with liquid electrolytes [9]. Very recently, the $SnS–P_2S_5$ amorphous materials were synthesized by mechanical milling and applied as an electrode to all-solid-state cells with the $Li_2S–P_2S_5$ solid electrolyte [10]. Because of using a common P_2S_5 component, a continuous sulfide network between electrode and electrolyte was formed in the cells.

In the present study, amorphous electrode materials of the $80SnS·20P_2S_5$ (mol%) and SnS were prepared by a mechanical milling technique. The change on morphology of the materials with increasing milling period of time was investigated. All-solid-state cells were fabricated with the $SnS–P_2S_5$ electrode and the $Li_2S–P_2S_5$ electrolyte. The charge–discharge behavior of the all-solid-state cells was examined at different current densities. The cell performance with the $80SnS·20P_2S_5$ electrode was compared to that with the SnS electrode. The effects of the addition of a network

* Corresponding author.
E-mail address: hayashi@chem.osakafu-u.ac.jp (A. Hayashi).

0378-7753/$ – see front matter © 2005 Elsevier B.V. All rights reserved.
doi:10.1016/j.jpowsour.2005.03.056

former P_2S_5 to SnS on the cell capacity and cyclability are discussed.

2. Experimental

Reagent-grade crystals SnS (Koujyundo Chem., 99.9%) and P_2S_5 (Aldrich, 98%) were used as starting materials for sample preparation. The mechanical milling treatment was carried out for the batches (1 g) of the mixed materials of $80SnS{\cdot}20P_2S_5$ (mol%) in an alumina pot (45 ml) with 10 alumina balls (10 mm in diameter) using a high-energy planetary ball mill apparatus (Fritsch Pulverisette 7). The rotation speed was fixed at 370 rpm and all the processes were conducted at room temperature in a dry Ar-filled glove box.

X-ray diffraction measurements (Cu Kα) were performed using an XRD diffractometer (Shimadzu, XRD-6000). The milled samples were put on a glass substrate and a surface of the samples was covered with a polyimide thin film in order to protect the samples from an attack of oxygen and moisture. Morphologies of mechanically milled samples were investigated by a scanning electron microscope (SEM) (JEOL Model JSM-5300).

All-solid-state electrochemical cells were assembled as follows. The $80Li_2S{\cdot}20P_2S_5$ glass-ceramic with high ambient temperature conductivity of about 10^{-3} S cm^{-1} was used as a solid electrolyte. The glass-ceramic material was prepared by mechanical milling and subsequent crystallization at around 230 °C [11]. A composite material was obtained by mixing of the $80SnS{\cdot}20P_2S_5$ milled sample (42 wt.%), the glass-ceramic electrolyte (53 wt.%), and acetylene-black (5 wt.%) powders. The composite powder as a working electrode and the solid electrolyte powder were put together in a polycarbonate tube and then were pressed under 3700 kg cm^{-2} to obtain a bilayer pellet. A small piece of Li was put on an In foil to form a Li–In alloy foil. The Li–In alloy foil as a counter electrode was pressed under 2500 kg cm^{-2} on the obtained bilayer pellet. After releasing the pressure, the three-layer pellet was sandwiched by two stainless-steel disks as current collectors to form two electrodes cells. The cells were charged and discharged under current densities from 64 to 320 μA cm^{-2} at 25 °C in an Ar atmosphere.

3. Results and discussion

Fig. 1 shows XRD patterns of the $80SnS{\cdot}20P_2S_5$ samples prepared by mechanical milling for several hours. The pattern of SnS milled for 20 h is also shown in this figure. Diffraction peaks due to the crystals of SnS and P_2S_5 are observed in the powder mixture of $80SnS{\cdot}20P_2S_5$ without mechanical milling (0 h). As the milling period increases, the intensity of the SnS and P_2S_5 peaks decreases and the halo pattern becomes dominant. The peaks due to P_2S_5 disappear after milling for 1 h, and the peaks due to SnS almost disappear after milling for 20 h. The $80SnS{\cdot}20P_2S_5$ amorphous material

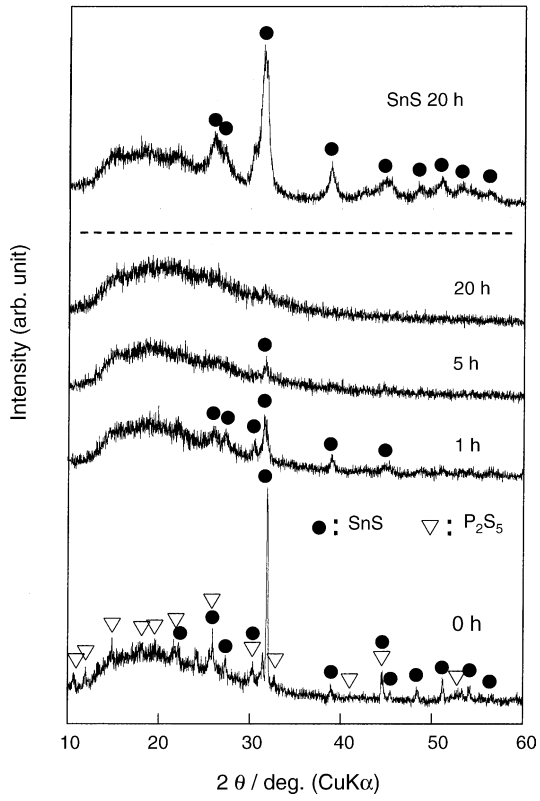

Fig. 1. XRD patterns of the $80SnS{\cdot}20P_2S_5$ (mol%) samples prepared by mechanical milling for several hours. The numbers in the figure denote the milling periods. The pattern of SnS milled for 20 h is also shown in this figure.

is obtained by mechanical milling for 20 h. On the other hand, the broad XRD peaks due to SnS still remain after milling the pure SnS crystal for 20 h, suggesting that it is very difficult to prepare amorphous SnS powders by milling. A glass former P_2S_5 added to SnS plays an important role in forming amorphous materials.

Morphologies of the milled powders were investigated by a scanning electron microscope (SEM). Fig. 2 shows the SEM photographs of the samples with the composition of $80SnS{\cdot}20P_2S_5$ at different milling periods: (a) 0 h, (b) 1 h, (c) 5 h, and (d) 20 h. As-mixed powders (a) consist of large SnS grains with over 100 μm in size and small P_2S_5 grains with below 20 μm in size. The large grains in 100 μm order disappear and aggregated domains consisting of a few micrometers grains are formed in the sample prepared by milling for 1 h (b). The morphology of the sample drastically changes in this period. After further milling over 1 h, the aggregated domains are pulverized and the size of grains gradually decreases with increasing milling periods; particles of a few micrometers in diameter are mainly obtained in the sample milled for 20 h (d).

The $80SnS{\cdot}20P_2S_5$ and SnS powders prepared by mechanical milling for 20 h were applied as a working electrode to all-solid-state cells. Fig. 3 shows the first charge–discharge curves of all-solid-state cells Li–In/$80SnS{\cdot}20P_2S_5$ and

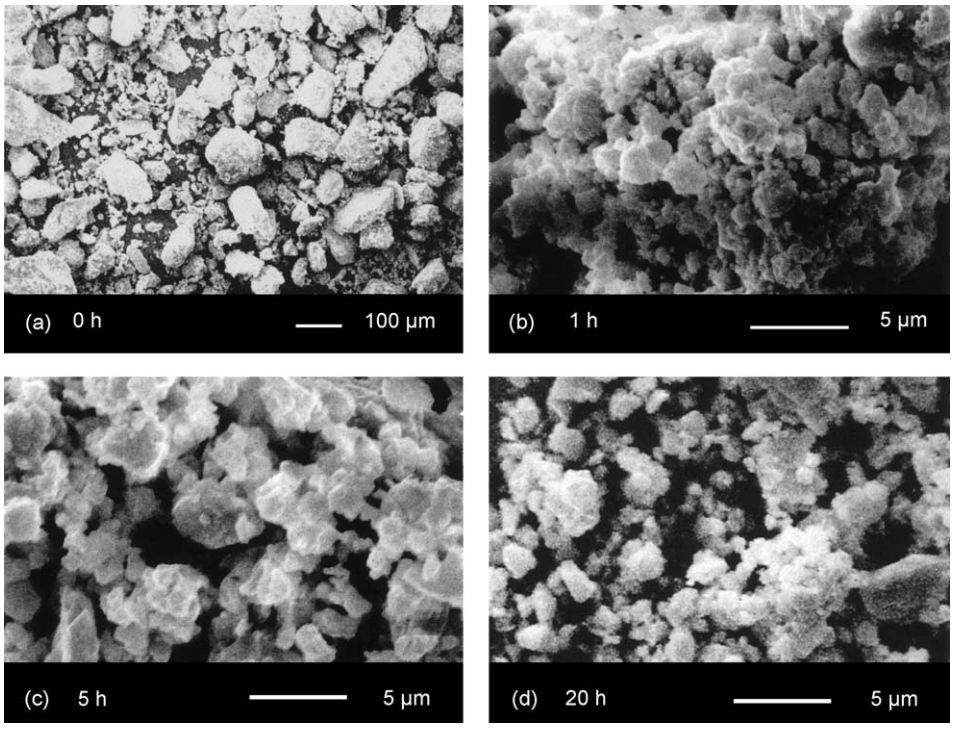

Fig. 2. SEM photographs of the samples with the composition of $80SnS{\cdot}20P_2S_5$ at different milling periods: (a) 0 h, (b) 1 h, (c) 5 h, and (d) 20 h.

Li–In/SnS. The $80Li_2S{\cdot}20P_2S_5$ glass-ceramic solid electrolyte with high conductivity was used in these cells. The charge–discharge measurements were carried out at a current density of 64 μA cm^{-2} at 25 °C. The ordinate on the left hand side denotes cell potential versus the Li–In counter electrode, and that on the right hand side denotes potential versus the Li electrode, which was calculated from the basis of the difference on the potential between Li–In and Li [12]. A cut-off voltage between 0 and 2 V versus Li was used. A charge corresponds to an insertion of lithium ions to the working electrode, while a discharge corresponds to an extraction of lithium ions from the working electrode.

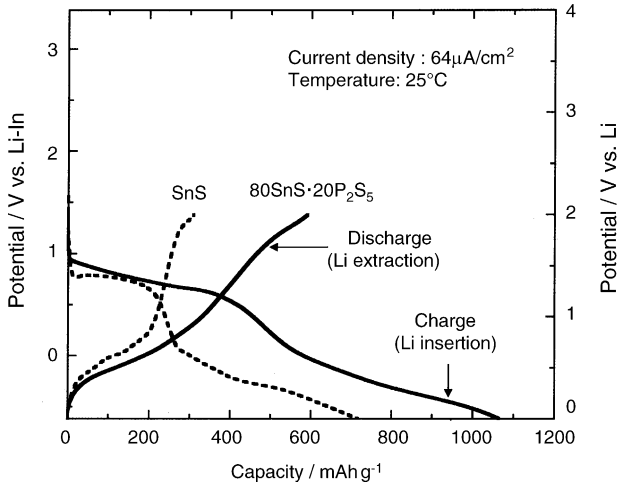

Fig. 3. Charge–discharge curves of all-solid-state cells Li–In/$80SnS{\cdot}20P_2S_5$ and Li–In/SnS at the 1st cycle. The $80Li_2S{\cdot}20P_2S_5$ glass-ceramic solid electrolyte with high conductivity was used in these cells. The charge–discharge measurements were carried out at a current density of 64 μA cm^{-2} at 25 °C.

Two plateaux at around 1.3 and 0.5 V (versus Li) are observed on the charge curve and one plateau at around 0.5 V is observed on the discharge curve in both cells. The $SnS–P_2S_5$ amorphous materials prove to work as electrode materials for all-solid-state rechargeable lithium batteries. The charge–discharge capacities of the cell with the $80SnS{\cdot}20P_2S_5$ electrode are larger than those with the SnS electrode. The former cell showed the charge capacity of 1070 mAh g^{-1} and the discharge capacity of 590 mAh g^{-1} while the latter cell showed the charge capacity of 720 mAh g^{-1} and the discharge capacity of 310 mAh g^{-1}. The discharge capacity of the cell with the $80SnS{\cdot}20P_2S_5$ electrode is 1.5 times as large as the capacity of conventional graphite anode materials used in commercialized lithium ion secondary batteries. The charge–discharge efficiency for the cell with the $80SnS{\cdot}20P_2S_5$ electrode is 56%, which is larger than that of the cell with SnS (43%). Although a large irreversible capacity is observed at the 1st cycle for the all-solid-state cells with $SnS–P_2S_5$ electrodes, the addition of P_2S_5 as a network former component to SnS enhances the reversible capacity of the cells.

The charge–discharge profiles of the all-solid-state cells with $SnS–P_2S_5$ electrodes are quite similar to those of the cells with $SnO–P_2O_5$ electrodes and conventional liquid electrolytes, although the potential of the first plateau on the

charge process is different. In the cell with $67SnO{\cdot}33P_2O_5$ glass as a working electrode, two plateaux at around 1.8 and 0.5 V (versus Li) were observed on the charge curve and one plateau at around 0.5 V was observed on the discharge curve [7].

The mechanism of electrochemical lithium insertion to SnO-based glassy materials has been widely investigated. The first plateau on the charge curve is due to the formation of metallic Sn nanoparticles ($Sn^{2+} \rightarrow Sn^0$) and Li_2O-based glassy matrix, and the second plateau is due to the formation of Li–Sn alloy domains ($Sn^0 \rightarrow$ Li–Sn) [2,3,13]. The former reaction is known to be irreversible and the formation of Sn is a main reason for the large irreversible capacity at the first cycle. The latter reaction is basically reversible and the formation of Sn (Li–Sn $\rightarrow Sn^0$) occurs on the discharge process.

Based on the charge–discharge process on SnO-based glasses, it is presumed that the first plateau of the cell with the $80SnS{\cdot}20P_2S_5$ electrode as shown in Fig. 3 is due to the formation of Sn nanoparticles and the Li_2S–P_2S_5 matrix. The formation of the highly Li^+ conductive Li_2S–P_2S_5 matrix around Sn active particles provides a close electrode–electrolyte interface, where smooth electrochemical reaction would occur during charge–discharge cycle. On the other hand, the Li_2S matrix would be formed in the cell with SnS electrode. The charge–discharge capacity of the cells with SnO-based electrodes is known to be affected by the size of Sn domains formed during lithium insertion. The agglomeration of Sn domains was inhibited and nano-sized Sn particles were present in SnO-based glasses, while the aggregation of particles occurred in crystalline SnO [2,3]. In the SnS-based electrodes, not only the size of Sn particles in the matrix but also the conductivity of the matrix would make a difference in the charge–discharge capacities of the cells as shown in Fig. 3.

Fig. 4 shows the cycling performance on discharge capacity for the all-solid-state cells using the $80SnS{\cdot}20P_2S_5$ and SnS electrodes. These cells can be repeatedly charged and discharged at a current density of 64 $\mu A\,cm^{-2}$ at room temperature. Although the discharge capacity gradually decreases with cycling in both the cells, the cells with the $80SnS{\cdot}20P_2S_5$ and SnS electrodes, respectively, maintain the capacity of over 400 and 270 $mAh\,g^{-1}$ even after 50 cycles. The addition of P_2S_5 as a glass former to SnS improves cell capacity and cyclability. After the measurements, the capacity drop is observed under the condition with higher current densities of 128 and 320 $\mu A\,cm^{-2}$. Since the capacity is recovered at the current density of 64 $\mu A\,cm^{-2}$ after several charge–discharge cycles at the higher current densities, the degradation of the SnS-based electrodes at higher current densities would not occur. Although the rate performance of the cells is not sufficient at the present stage, the SnS–P_2S_5 amorphous materials are the probable negative electrodes with high capacity for all-solid-state rechargeable lithium batteries.

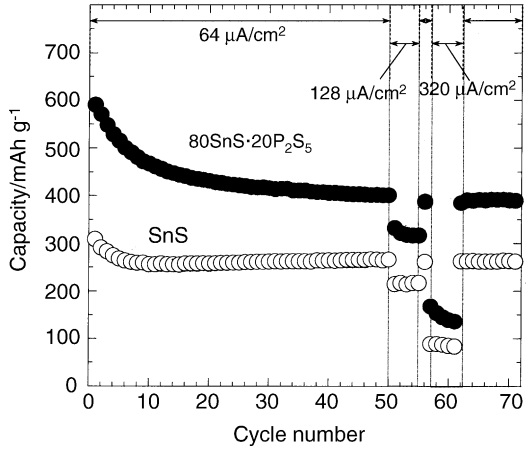

Fig. 4. Cycling performance on discharge capacity for the all-solid-state cells using the $80SnS{\cdot}20P_2S_5$ and SnS electrodes.

4. Conclusions

The $80SnS{\cdot}20P_2S_5$ amorphous material was prepared by mechanical milling for 20 h, while amorphous SnS was not prepared by milling for the same period. All-solid-state cells with the SnS–P_2S_5 amorphous electrode and the Li_2S–P_2S_5 glass-ceramic electrolyte exhibited high reversible capacity of over 400 $mAh\,g^{-1}$ for 50 cycles at room temperature. The capacity and cyclability of the cell with the $80SnS{\cdot}20P_2S_5$ electrode were higher than those with the SnS electrode. The P_2S_5 component added to the SnS active material played an important role in enhancing the availability of SnS.

Acknowledgements

This work was supported by the Grant-in-Aid for Scientific Research on Priority Areas from the Ministry of Education, Culture, Sports, Science and Technology of Japan.

References

[1] Y. Idota, T. Kubota, A. Matsufuji, Y. Maekawa, T. Miyasaka, Science 276 (1997) 1395.
[2] I.A. Courtney, J.R. Dahn, J. Electrochem. Soc. 144 (1997) 2943.
[3] G.R. Goward, L.F. Nazar, W.P. Power, J. Mater. Chem. 10 (2000) 1241.
[4] M. Nakai, A. Hayashi, H. Morimoto, M. Tatsumisago, T. Minami, J. Ceram. Soc. Jpn. 109 (2001) 1010.
[5] H. Morimoto, M. Tatsumisago, T. Minami, J. Electrochem. Soc. 146 (1999) 3970.
[6] A. Hayashi, M. Nakai, H. Morimoto, T. Minami, M. Tatsumisago, J. Mater. Sci. 39 (2004) 5361.
[7] A. Hayashi, T. Konishi, M. Nakai, H. Morimoto, K. Tadanaga, T. Minami, M. Tatsumisago, J. Ceram. Soc. Jpn. 112 (2004) 695.

[8] F. Mizuno, S. Hama, A. Hayashi, K. Tadanaga, T. Minami, M. Tatsumisago, Chem. Lett. (2002) 1244.
[9] T. Momma, N. Shiraishi, A. Yoshizawa, T. Osaka, A. Gedanken, J. Zhu, L. Sominski, J. Power Sources 97/98 (2001) 198.
[10] A. Hayashi, T. Konishi, K. Tadanaga, T. Minami, M. Tatsumisago, submitted for publication.
[11] A. Hayashi, S. Hama, T. Minami, M. Tatsumisago, Electrochem. Commun. 5 (2003) 111.
[12] K. Takada, N. Aotani, K. Iwamoto, S. Kondo, Solid State Ionics 86–88 (1996) 877.
[13] A. Hayashi, M. Nakai, M. Tatsumisago, T. Minami, M. Katada, J. Electrochem. Soc. 150 (2003) A582.